ACS Catalysis

Research Article

pubs.acs.org/acscatalysis

Adsorption and Reaction of Acetaldehyde on Shape-Controlled CeO_2 Nanocrystals: Elucidation of Structure–Function Relationships

Amanda K. P. Mann, Zili Wu, Florencia C. Calaza,† and Steven H. Overbury*

Chemical Sciences Division and Center for Nanophase Materials Sciences, Oak Ridge National Laboratory, Oak Ridge, Tennessee 37831, United States

Supporting Information

ABSTRACT: CeO_2 cubes with {100} facets, octahedra with {111} facets, and wires with highly defective structures were utilized to probe the structure-dependent reactivity of acetaldehyde. Using temperature-programmed desorption (TPD), temperature-programmed surface reactions (TPSR), and *in situ* infrared spectroscopy, it was determined that acetaldehyde desorbs unreacted or undergoes reduction, coupling, or C–C bond scission reactions, depending on the surface structure of CeO_2. Room-temperature FTIR indicates that acetaldehyde binds primarily as η^1-acetaldehyde on the octahedra, in a variety of conformations on the cubes, including coupling products and acetate and enolate species, and primarily as coupling products on the wires. The percent consumption of acetaldehyde ranks in the following order: wires > cubes > octahedra. All the nanoshapes produce the coupling product crotonaldehyde; however, the selectivity to produce ethanol ranks in the following order: wires ≈ cubes ≫ octahedra. The selectivity and other differences can be attributed to the variation in the basicity of the surfaces, defects densities, coordination numbers of surface atoms, and the reducibility of the nanoshapes.

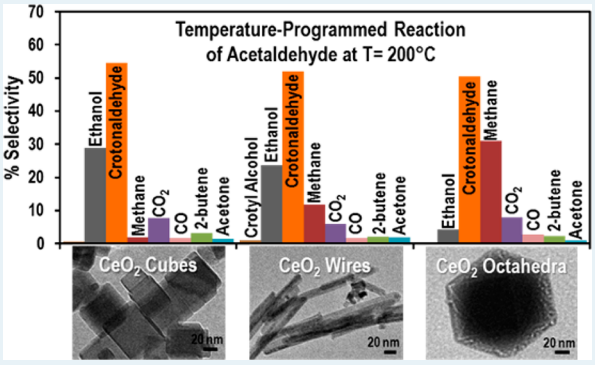

KEYWORDS: *CeO_2 nanoshapes, structure dependence, acetaldehyde reaction, DRIFTS, temperature-programmed reaction, Aldol condensation, Cannizzaro disproportionation*

INTRODUCTION

Cerium oxide (CeO_2) has been shown to be an attractive material for many applications, because of its oxygen storage capability, rich redox chemistry, versatile acid and base catalytic chemistry, and relative abundance. For example, it is an important component in three-way catalytic converters,[1] water–gas shift reactions,[2] oxygen sensors,[3,4] and fuel cells.[5] In addition, it has been found to promote several organic reactions,[6] including ethanol oxidation,[7] decomposition of formic acid,[8,9] and CO oxidation.[10]

Previously, experiments have shown that CeO_2 is an active catalyst to promote the coupling of acetaldehyde, an oxygenate species, to form several products including crotonaldehyde, crotyl alcohol, butane, butadiene, and acetone.[11,12] Oxygenates have garnered much attention as fuel additives, as components obtained from the processing of biomass, and as an intermediate for value-added products.[13] However, the conversion of oxygenates upon catalysis is not well-understood. It is of critical importance to optimize these catalytic transformations, and this goal requires detailed, fundamental studies of structure–activity relationships using well-defined catalysts. For example, oxygenate species derived from the processing of biomass often require the removal of oxygen via breakage of C–O bonds without scission of C–C bonds to generate valuable products.[14,15] In order to understand and optimize these selective conversions, fundamental studies of model systems are required. Acetaldehyde is of particular interest as a model oxygenate compound, as it can undergo acid- or base-catalyzed coupling reactions to produce higher-molecular-weight species, forming value-added products. Still, there remains a need to evaluate the influence of various shape-dependent properties on catalytic performance to provide information that can guide the design of more active and selective catalysts.

To this end, experiments have been performed probing the adsorption and reaction of acetaldehyde on $CeO_2(111)$ and $CeO_2(100)$ single-crystal thin films.[16−18] It was found that these two faces vary with respect to the initial adsorption of acetaldehyde and the resulting desorption products. Acetaldehyde primarily binds in a μ-C,O-conformation on $CeO_2(100)$ facets, and in a η^1-conformation on $CeO_2(111)$.[16−18] Reactivity also varies considerably between the different surface terminations. $CeO_2(100)$ evolves unreacted acetaldehyde, CO_2, CO, acetylene, H_2O, and trace amounts of crotonaldehyde, while $CeO_2(111)$ facets simply desorb unreacted acetaldehyde. In addition, reduction of the ceria surface (to

Received: May 5, 2014
Revised: June 10, 2014
Published: June 12, 2014

   dx.doi.org/10.1021/cs500611g | ACS Catal. 2014, 4, 2437−2448

CeO_{2-x}) alters the reactivity and results in the evolution of different products. Nevertheless, the reactivity of single-crystalline films is typically studied by temperature-programmed desorption (TPD) under ultrahigh vacuum (UHV) conditions and the question remains whether these results can be extrapolated to practical reactor conditions.

Syntheses have been reported to form CeO_2 nanoparticles[19] and shape-controlled nanocrystals,[20−22] as well as various other architectures.[22−25] Here, nanosized CeO_2 in the form of cubes, wires, and octahedra generated via a hydrothermal method are used to probe the catalytic adsorption and reaction of acetaldehyde on well-defined CeO_2 surfaces. CeO_2 cubes expose {100} facets and octahedra expose {111} facets. CeO_2 {111} facets have been calculated to be the most thermodynamically stable surface termination.[26] CeO_2 wires or rodlike structures are commonly thought to expose a combination of {110} + {100} facets.[21,27,28] However, recent results suggest that, depending on the annealing treatment, CeO_2 wires and rods could actually expose a variety of facets, including {111} facets, and possess large numbers of nanoscopic structural defects.[29] Here, the structure of the CeO_2 wires will be referred to as a defect structure. CeO_2 is known to possess strong basic sites and weaker acidic sites.[6] The geometry of the surface affects the positions and coordination numbers of available acid and base sites, thereby modifying the reactivity. The calculated oxygen-vacancy formation energies are expected to follow the order of (110) < (100) < (111), and is anticipated to influence the adsorption motifs for molecules on their surfaces and redox activity.[7,10,21,30−32]

Therefore, the adsorption and reaction of acetaldehyde on CeO_2 cubes, wires, and octahedra are expected to exhibit shape-dependent properties, resulting in diverse reactivity and selectivity. TPD, diffuse reflectance infrared spectroscopy (DRIFTS), and isothermal and temperature-programmed surface reaction (TPSR) methods have been utilized to determine reaction intermediates, products, and selectivities, as well as to propose reaction pathways. Importantly, it was found that crotonaldehyde is the dominant coupling product for all nanoshapes; however, the selectivity to this product, as well as the overall conversion of acetaldehyde, differs between the various nanoshapes. These results contribute to a detailed fundamental understanding of structure−reactivity relationships and provide insight into the design and production of advanced catalysts.

EXPERIMENTAL SECTION

Materials. All chemicals were handled in air and used as received. $Ce(NO_3)_3{\cdot}6H_2O$ (99%) was purchased from Sigma−Aldrich. NaOH (≥97%) and HNO_3 (68%) was purchased from Fisher Scientific. NH_4OH (28−30%) was purchased from Acros Organics. Deionized water (18.2 MΩ) was used in all syntheses. Acetaldehyde (0.5% or 5000 ppm) in helium was purchased from Air Liquide America L.P.

CeO_2 Octahedra. A quantity of 0.868 g of $Ce(NO_3)_3{\cdot}6H_2O$ (0.002 mol) was dissolved in 80 mL of H_2O. The solution was heated at 190 °C without stirring for 6 h in a 100 mL quartz-lined stainless steel homemade autoclave reactor, and the pressure reached 14−14.5 bar. The resulting products were allowed to cool to room temperature, dispersed in 10 mL of ethanol, and isolated via centrifugation. The products were then dispersed in 10 mL of warm DI water and isolated via centrifugation. This washing procedure was repeated two more times. The octahedra were dried under vacuum overnight and then calcined at 400 °C for 4 h in air. It should be noted that the product particles were a combination of discrete and agglomerated octahedra. The octahedra have a surface area of 10 m^2/g. SEM and XRD of the octahedra are shown in Figure S1 in the Supporting Information.

CeO_2 Cubes and Wires. CeO_2 cubes and wires were prepared based on a method published previously with some modifications.[27] Briefly, 0.434 g of $Ce(NO_3)_3{\cdot}6H_2O$ (0.001 mol) was dissolved in 2.5 mL of H_2O. Then, 4.8 g of NaOH (0.120 mol) was dissolved in 17.5 mL of H_2O and added to the $Ce(NO_3)_3$ solution. Upon the addition of NaOH solution, an opaque precipitate formed, indicating hydrolysis of $Ce(NO_3)_3$ and the formation of colloidal $Ce(OH)_3$. The solutions were heated to 90 or 180 °C for 24 h for the wires and cubes, respectively, without stirring, in a 50-mL Teflon-lined stainless steel 4871 Parr reactor. The pressure reached ∼0.5 bar for the wires and ∼7 bar for the cubes. The resulting products were allowed to cool to room temperature, dispersed in 10 mL of ethanol, and isolated via centrifugation. The products were then dispersed in 10 mL of warm DI water and isolated via centrifugation. This washing procedure was repeated two more times. The products were dried under vacuum overnight at 100 °C. The removal of Na impurities is important, since previous studies have shown that ion impurities can affect the reactivity of CeO_2.[33] Na impurities were removed by dispersing the products in 2 mL of 0.1 M NH_4OH, which was suspended in an ultrasonic bath for 2 min. The product was isolated via centrifugation, followed by three warm water washes. The products were then dispersed in 2 mL of 0.1 M HNO_3, which was suspended in an ultrasonic bath for 2 min. The product was isolated via centrifugation, followed by three warm water washes. The products were dried under vacuum overnight, and then calcined at 400 °C for 4 h in air. The cubes and wires have surface areas of 17 and 71.5 m^2/g, respectively. SEM and XRD of the cubes and wires are shown in Figure S1 in the Supporting Information.

Characterization. Cerium oxide samples were characterized by many techniques. Scanning electron microscopy (SEM) was performed using a Zeiss Merlin system operating at 5 kV. Transmission electron microscopy (TEM) was performed using a Zeiss Libra 120 system operating at 120 kV. Powder X-ray diffraction (XRD) was performed on a Panalytical X'Pert Pro system, using Cu Kα radiation. Three-point Brunauer−Emmett−Teller (BET) analysis of N_2 adsorption isotherms was employed to obtain surface area measurements using a Micromeretics Gemini system.

Temperature-Programmed Desorption (TPD). Acetaldehyde TPD was performed on a temperature-controlled plug-flow reactor (Altamira, Model AMI-200) coupled to a downstream gas sampling quadrupole mass spectrometer (QMS, Pfeiffer-Balzer Omnistar). Enough catalyst was loaded in a U-shaped quartz tube (4 mm I.D.) supported by quartz wool to equal a surface area of 1.43 m^2 of the respective samples (i.e., 0.020 g wires, 0.0841 g cubes, 0.143 g octahedra) and quartz sand was added to make the approximate volumes equivalent. All samples were pretreated by heating to 400 °C (10 °C/min) and holding for 1 h in a gas stream of 5% O_2/He (30 sccm). The samples were then cooled to room temperature, followed by purging in a gas stream of He (30 sccm). A gas stream of 0.5% acetaldehyde/He (Air Liquide, 5000 ppm acetaldehyde) (30 sccm) was flowed over the sample for 10 min, followed by a gas stream of He (30 sccm) for 10 min. The temperature was then ramped to 400 °C (3 °C/min) under a gas stream of He (30 sccm). Because the cracking fragments for acetaldehyde and the products have considerable overlap in the mass spectrum, the analysis required that QMS mass intensities be corrected. This correction was performed as described previously,[7] by creating a matrix containing the mass fragment intensities for each product (acetaldehyde, H_2, methane, H_2O, CO, ethanol, O_2, CO_2, 1,3-butadiene, 2-butene, crotyl alcohol, acetone, furan, crotonaldehyde, benzene, and toluene) contributing to the masses of 2, 15, 18, 28, 29, 31, 32, 44, 54, 56, 57, 58, 68, 70, 78, and 90 and solving the resulting equation to convert mass intensity to product yield (partial pressure). The mass fragment intensities were corrected for QMS sensitivity parameters, including ionization efficiency, quadrupole transmissions, and multiplier gain, as described previously.[24] To determine TPD yields, each product partial pressure was measured over the entire temperature (time) range of the TPD experiment for each desorption product. TPD carbon selectivity was obtained from eq 1, where Y_i is the *temperature-integrated* partial pressure, n_i is the carbon number in each product, and the sum is over all analyzed desorption products, including acetaldehyde.

dx.doi.org/10.1021/cs500611g | ACS Catal. 2014, 4, 2437−2448

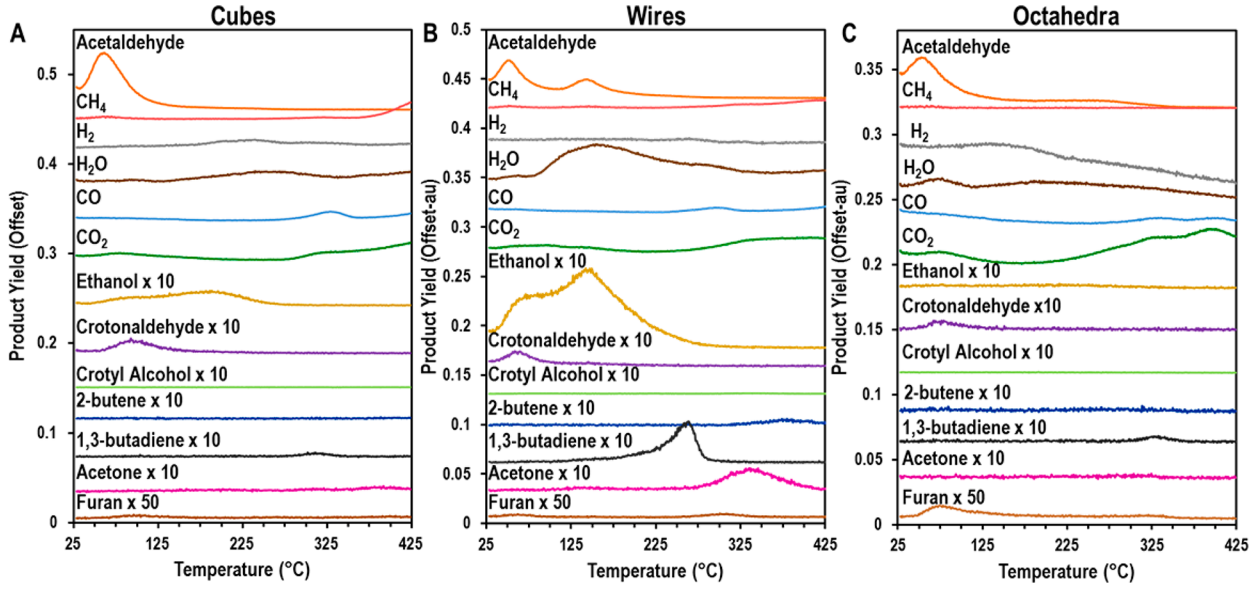

Figure 1. Temperature-programmed desorption mass spectrum profiles showing the characteristic mass fragments of different products resulting from the room-temperature adsorption of acetaldehyde followed by heating in He for CeO_2: (A) cubes, (B) wires, and (C) octahedra. The profiles are offset vertically and multiplied as indicated for clarity.

$$S_i\ (\%) = \frac{100 \times (Y_i n_i)}{\sum_{\text{products}} Y_j n_j} \quad (1)$$

Temperature-Programmed Surface Reaction (TPSR). The same reactor, catalyst amounts, and pretreatment conditions as those for TPD were used for TPSR. A gas stream of 0.5% acetaldehyde/He (30 sccm) was flowed over the sample for 10 min at room temperature, and then the temperature was ramped to 400 °C at 3 °C/min. The product gas stream was sampled continuously using the QMS and the data was corrected for overlaps and QMS sensitivity using the same methods described above to calculate the temperature (time)-dependent product yield. Selectivity at each temperature was obtained from these yields and computed from eq 1, where the sum is over all components *except* acetaldehyde.

Conversion during Isothermal Reaction. The same reactor, catalyst amounts, and pretreatment conditions as those for TPD were used for isothermal reactions, except that after pretreatment in 5% O_2/He, the samples were cooled in He to a specified reaction temperature. Then a gas stream of 0.5% acetaldehyde/He (30 sccm) was flowed over the sample and 1 mL aliquots of the product gas stream was collected periodically using an automatic sampling valve and analyzed using a Buck Scientific gas chromatograph (GC) with a 2-m packed 15% Carbowax 20 M column (2.0 mm O.D., $^1/_8$-in. I.D.), a thermal conductivity detector (TCD), and a flame ionization detector (FID). The product peak areas obtained from the GC were integrated to determine the yield of each product based on calibration standards. Acetaldehyde consumption was obtained from the measured acetaldehyde eluted compared to the inlet acetaldehyde measured while bypassing the reactor. Product selectivity was determined from eq 1 where the sum is over all observed eluted species *including* acetaldehyde. The carbon capture was deduced from the amount of acetaldehyde consumed and the carbon-corrected yield of products evolved at each temperature.

Surface Adsorbates by Fourier Transform IR (FTIR) Spectroscopy. FTIR spectroscopy was conducted in a diffuse reflectance cell (Pike Technologies, Model HC-900, cell volume of ~6 cm^3) in a Nicolet Nexus 670 FTIR spectrometer using a MCT/A detector with a spectral resolution of 4 cm^{-1}. A background spectrum was collected using 256 scans at room temperature after the sample was pretreated. Diffuse reflectance FTIR spectroscopy (DRIFTS) spectra were collected by subtracting out the background from the resulting spectra. Gases leaving the reaction cell were analyzed downstream using a gas sampling quadrupole mass spectrometer (QMS, Pfeiffer–Balzer Omnistar). Cerium oxide samples were pretreated by heating to 400 °C (10 °C/min) and holding for 1 h in a gas stream of 5% O_2/He (25 sccm). The samples were then cooled to room temperature, and then purged in a gas stream of He (25 sccm). A pulse of 0.5% acetaldehyde/He (sample loop 0.5 mL) was introduced to the sample and continuous spectra (16 scans each) were collected over 5 min. Then, a gas stream of 0.5% acetaldehyde/He (25 sccm) was flowed over the sample for 2 min, followed by a gas stream of He (25 sccm) for 2 min. The temperature was then ramped to 400 °C (10 °C/min) and the resulting temperature-programmed DRIFTS spectra (TP-DRIFTS) were recorded throughout.

RESULTS

Temperature-Programmed Desorption (TPD). The product profiles resulting during TPD of adsorbed acetaldehyde on CeO_2 nanoshapes are shown in Figure 1. Here, major, minor, and trace products are classified as products that comprise >5%, 1%–5%, and <1% of the carbon-containing product stream normalized to their carbon number over the entire temperature range, as monitored by mass spectrometry during TPD, respectively, and are highlighted in Table S1 in the Supporting Information. Details can be found in the Experimental Section. For all CeO_2 nanoshapes, acetaldehyde is a major desorption product and is observed between 30 °C and 140 °C. Desorption of CO_2, CO, H_2O, and H_2 from all nanoshapes indicates that decomposition is a prevalent pathway. Water is favored over H_2 for the wires, but they are comparable for the cubes and octahedra. The broad, non-correlated desorption ranges are indicative of complex stepwise processes, leading to these desorption products that vary between the shapes.

Of greater interest are the other carbon carrying products. Crotonaldehyde, formed by Aldol condensation, is a minor product that is also desorbed in this temperature region. A trace amount of furan is observed on the octahedra between 50 °C and 100 °C. For the wires, a second acetaldehyde peak is observed between 110 °C and 180 °C. Ethanol, formed via a Cannizzaro disproportionation reaction shown in Scheme 1,[34] is a major product on the wires and a minor product on the

dx.doi.org/10.1021/cs500611g | ACS Catal. 2014, 4, 2437–2448

Scheme 1. Proposed Mechanism for the Formation of Acetate and Ethoxide from the Cannizzaro Reaction Involving a Vacancy and Surface Oxygen for Example on a CeO_2{111} Facet (Not to Scale)[a]

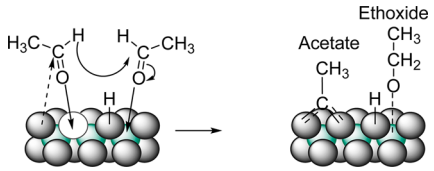

[a]Green spheres represent Ce atoms, gray spheres represent O atoms, and white circles denote oxygen vacancies.

cubes below 275 °C, but is only observed as a trace product for the octahedra. 1,3-Butadiene, which is formed by reductive coupling, is observed on all nanoshapes, as a trace product on the octahedra and cubes between 290 °C and 360 °C, and as a minor product at lower temperatures on the wires between 125 °C and 300 °C. Crotyl alcohol, a coupling product derived from the reduction of crotonaldehyde, is only evolved in trace amounts on the wires. In addition, another reductive coupling product, 2-butene, is only observed in trace amounts, primarily on the wires above 325 °C. Finally, products formed from the scission of C−C bonds (CO, CO_2, methane, and acetone) are only observed at higher temperatures. Acetone, which has been proposed to form from two acetate groups undergoing ketonization,[11] is evolved from the wires and cubes as a minor product above 275 °C, but as a trace product on the octahedra. Methane is evolved as a major product above 350 °C on the cubes and above 300 °C on the wires, but as a minor product on the octahedra. CO and CO_2 are evolved from all nanoshapes above ∼270 °C as major products.

Summarizing, the various nanoshapes had different selectivities for the coupling products. All nanoshapes produced the coupling product crotonaldehyde; however, the wires and cubes additionally produce 1,3-butadiene and/or acetone as minor products. Wires and cubes also desorbed acetaldehyde, and its reduced form, ethanol. In comparison, the octahedra primarily desorb acetaldehyde as a major product, and only trace amounts of its reduced form, ethanol. The amount of ethanol desorbed was greatest on the wires.

Surface Adsorbates via TP-DRIFTS. DRIFTS spectra obtained after flowing acetaldehyde at room temperature over the different catalyst nanoshapes, followed by helium flow to remove gas phase and weakly adsorbed acetaldehyde, are shown in Figure 2. Table 1 shows the corresponding peak assignments. All samples exhibited bands at room temperature in the 3000−2800 cm^{-1} region and are assigned to symmetric and asymmetric $\nu(CH_3)$ and $\nu(CH_2)$ modes. Bands in the 1720−1704 cm^{-1} can be assigned to $\nu(C{=}O)$ mode of η^1-acetaldehyde.[16,35] Notably, the band in this region on the wires is a very weak shoulder, compared to the strong band observed on the cubes and the octahedra. Many of the bands observed at room temperature correlate to species other than acetaldehyde. All the nanoshapes show bands that can be assigned to red-shifted $\nu(C{=}O)$ and $\nu(C{=}C)$ modes that likely correlate to coupling products that form at room temperature. For example, the coupling product crotonaldehyde is observed to desorb at low temperatures in TPD experiments. Coupling products also contribute to the $\nu(CH_3)$ and $\nu(CH_2)$ modes. These $\nu(C{=}C)$ and $\nu(C{=}O)$ bands are the dominant surface species on the wires. Though the small broad band at 1629 cm^{-1} on the cubes

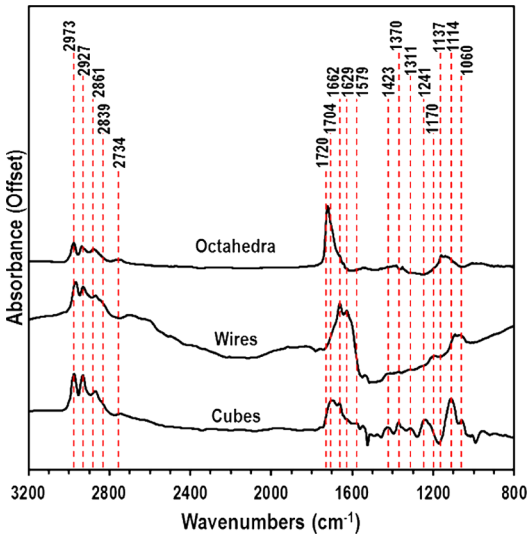

Figure 2. Room-temperature DRIFTS spectra for CeO_2 cubes, wires, and octahedra after 2 min of acetaldehyde flow, followed by 2 min of helium flow.

is assigned to coupling products, together with the band at 1311 cm^{-1}, it could also correspond to an enolate species,[36] which is not observed on the wires or octahedra at room temperature. Enolate is expected to be the primary intermediate to form coupling products via Aldol addition.[16]

Broad bands at 1579 and 1423 cm^{-1} on the cubes are assigned to $\nu_{as}(O{-}C{-}O)$ and $\nu_s(O{-}C{-}O)$ of acetate.[7,11] However, the room-temperature band on the cubes at 1579 cm^{-1} is sufficiently broad that it could also correspond to $\nu_{as}(O{-}C{-}O)$ of a carbonate moiety. It often is difficult to distinguish between acetate and carbonate groups by FTIR. If the peak at 1579 cm^{-1} also correlates to a carbonate species, the band at 1241 cm^{-1} can then be assigned to $\nu_s(O{-}C{-}O)$. The split of ∼340 cm^{-1} indicates that the carbonate is bound in a bidentate conformation.[37] In contrast to the cubes, no acetate bands are observed on the wires or octahedra at room temperature. The bands at 1114 and 1060 cm^{-1} on the cubes, 1094 and 1069 cm^{-1} on the wires, and the broad band at 1137 cm^{-1} on the octahedra are assigned to the binding of monodentate and bidentate $\nu(C{-}O)$ ethoxide species, as represented in Scheme S1 in the Supporting Information. Idriss and co-workers identified ethoxy species upon adsorption of acetaldehyde on CeO_2 at room temperature.[11] Previous experiments of ethanol adsorption showed bands at 1050 cm^{-1} for bidentate and 1120 and 1096 cm^{-1} for monodentate species.[7]

TP-DRIFTS profiles measured as a function of increasing temperature in helium are shown in Figure 3 for the various CeO_2 nanoshapes. The room-temperature band at 1704 cm^{-1} on the cubes and wires and 1720 cm^{-1} on the octahedra corresponding to η^1-acetaldehyde disappears as acetaldehyde desorbs and the peak is largely gone by 100 °C on the cubes and wires, and 150 °C on the octahedra. The bands correlating to acetate species on the cubes become more prominent as the temperature is increased, indicating that the amount of acetate on the surface is increasing. Very small acetate bands begin to grow on the octahedra above 100 °C at 1509 and 1432 cm^{-1}. Notably, acetate is not observed on the wires, even as the temperature increases to 350 °C. Acetate groups can form upon oxidation of acetaldehyde by the CeO_2 surface or by a

dx.doi.org/10.1021/cs500611g | ACS Catal. 2014, 4, 2437−2448

Table 1. Vibrational Assignments for Observed IR Peaks from the Adsorption of Acetaldehyde on CeO_2 Nanoshapes

vibrational mode	Vibrational Assignments (cm^{-1})			
	acetaldehyde on CeO_2[a]	cubes	wires	octahedra
$\nu_{as}(CH_3)$	3002, 2969, 2965	2979	2964	2978
$\nu_{as}(CH_2)$	2964, 2925	2923	2927	2934
$\nu_s(CH_3)$	2918, 2864	2871	2867	2877
$\nu_s(CH_2)$	2836	2839 (shoulder)	2837 (shoulder)	N/O
ν(CH) η^1-acetaldehyde	2760−2746, 2759	2745	N/O	2734
ν(C═O) η^1-acetaldehyde	1723	1704	1704 (weak shoulder)	1720
ν(C═O) and (C═C) coupling products	1656, 1642, 1630	1666, 1629	1662, 1629	1660 (shoulder), 1643
ν_{as}(OCO) acetate and bidentate carbonate	1584, 1611, 1565	1579 (broad)	N/O	1592
ν(C═C) enolate	1600	1629	N/O	N/O
ν_s(OCO) acetate	1443, 1429, 1406, 1422	1423	N/O	1407
$\delta_s(CH_3)$	1380, 1365	1371	N/O	N/O
$\delta(CH_2)$ enolate	1317	1311	N/O	N/O
ν_s(OCO) bidentate carbonate	1269, 1260	1241	N/O	N/O
ν(C−O) monodentate	1134, 1120, 1096	1114	1094	1137, 1120
ν(C−O) bidentate	1050, 1028	1060	1069	N/O

[a]Data taken from refs 7, 16, 38, and 56.

Cannizzaro disproportionation reaction. The carbonate bands at 1579 and 1241 cm^{-1} on the cubes grow as temperature increases, suggesting that the amount of carbonate on the surface increases. Peaks at 1592 and 1210 cm^{-1} grow in on the octahedra above 200 °C and likely correspond to the formation of bidentate carbonate species. However, no carbonate species are observed on the wires. Enolate bands that are observed on the cubes at 1629 and 1311 cm^{-1} are gone by 200 °C, but do not obviously correspond to evolution of any product. Instead, the enolate moiety likely reacts to form some other more-stable surface species (e.g., acetate).

The bands for bidentate ethoxide ν(C−O) seen at room temperature on all the nanoshapes show varying trends. On the octahedra, the band is small initially and is gone by 150 °C; however, only trace amounts of ethanol evolve in TPD. In contrast, for the cubes, the ethoxide bands decrease up to 200 °C, but never fully disappear and correlate to the evolution of ethanol in the TPD below 225 °C as a minor product. On the wires, the bands for bidentate ν(C−O) show a small decrease below 250 °C. In the TPD, ethanol is observed as a major product on the wires below 250 °C. On the cubes, wires, and octahedra, stretches associated with ν(C═C) and/or ν(C═O) increase sharply up to 200, 250, and 100 °C, respectively, and could indicate the formation of coupling products. On the cubes, these bands begin to decrease while 1,3-butadiene is evolved from 280 °C to 360 °C in TPD. The bands associated with coupling products on the wires begin to decrease up to 350 °C. In TPD, 1,3-butadiene is evolved between 125 °C and 250 °C, and above 300 °C, 2-butene is evolved on the wires. 1,3-Butadiene is desorbed in TPD on the octahedra from 300 °C to 375 °C. The bands associated with coupling products on the octahedra begin to decrease by 150 °C. Peaks associated with coupling products are largely gone on the octahedra and cubes by 350 °C, but persist on the surface of the wires. On the cubes and wires, a stretch in the aromatic region appears above 250 °C at 3037 cm^{-1} for the cubes and above 150 °C at 3020 cm^{-1} for the wires. While no aromatic compounds are observed at high temperatures in TPD, this could be because too little is evolved to be detected. As will be discussed later, in TPSR, benzene and toluene are observed; this band could be the surface species relating to these types of products.

Finally, bands at ∼2975 and 2870 cm^{-1}, corresponding to $\nu(CH_3)$ modes, disappear at high temperatures on all the nanoshapes as acetaldehyde and coupling products (e.g., crotonaldehyde, acetone) are desorbed. However, bands corresponding to $\nu(CH_2)$ modes at ∼2925 and 2839 cm^{-1} are maintained up to 350 °C on the cubes and wires. These are likely coupling products and coke and indicate that deactivation of the catalyst is a concern. Higher reaction temperatures may be able to promote the reaction and subsequent desorption of these surface species, especially as the oxygen mobility increases at high temperature; however, heating to temperatures above 450 °C has been shown to induce morphological changes on the cubes and wires. In general, little remains on the surface of the octahedra at 350 °C, compared to the other nanoshapes, indicating that most of the acetaldehyde and its products have desorbed.

Temperature-Programmed Surface Reaction (TPSR). TPSR profiles for the various nanoshapes under a flow of 0.5% acetaldehyde in helium at 30 sccm are shown in Figure 4. In general, there are two main regions observed in the TPSR. First, there is the low-temperature region, $T < T_{10}$, where the consumption of acetaldehyde is <10%. T_{10} is ∼375 °C for the cubes and ∼315 °C for the wires and octahedra, and this temperature is indicated by a dashed red line in Figure 4. Primarily, acetaldehyde, disproportionation, and coupling products are observed at $T < T_{10}$. Second, at $T > T_{10}$, the acetaldehyde consumption increases abruptly, so a larger amount of products, including C_1 products, are observed.

For all nanoshapes, unconverted acetaldehyde is the major carbon-containing component detected in the product stream when $T < T_{10}$. However, there are many differences in the product distribution and their variation with temperature, which is dependent on the catalyst morphology. Figure 5 compares the product selectivities of the carbon-containing products (see the Experimental Section) at 200 °C extracted from the TPSR data, and similar results for other temperatures are shown in Figure S2 in the Supporting Information. From Figure 4, it can be seen that significant amounts of ethanol are produced on the cubes and wires, and their profiles differ. However, ethanol is formed beginning at room temperature on both shapes; the cubes have a maximum formation rate at 180 °C, whereas the wires have multiple maxima, including at 60

dx.doi.org/10.1021/cs500611g | ACS Catal. 2014, 4, 2437−2448

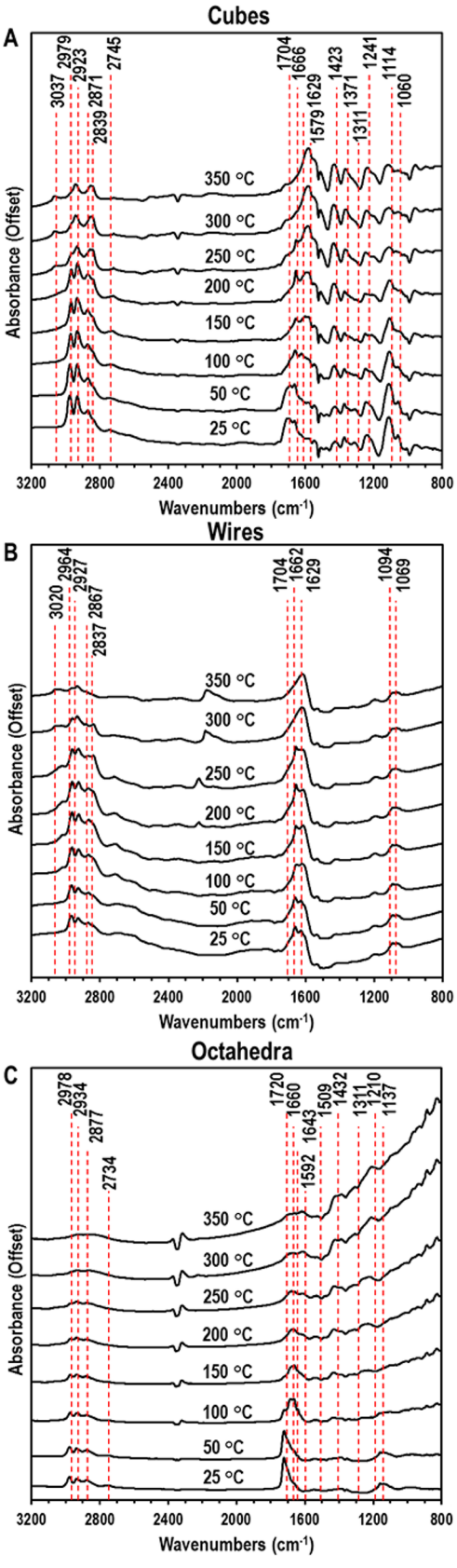

Figure 3. TP-DRIFTS spectra recorded in He following the room-temperature adsorption of acetaldehyde on CeO_2: (A) cubes, (B) wires, and (C) octahedra.

and 235 °C. The selectivity to form ethanol for both is ∼25% at 200 °C. In contrast, only a small amount of ethanol is evolved from the octahedra, with a selectivity of <5% at 200 °C.

Crotonaldehyde is evolved from all three nanoshapes, and is the dominant coupling product detected. Crotonaldehyde formation starts ∼30 °C higher for the cubes and octahedra than for the wires. Production is almost constant from 200 °C up to $T > T_{10}$ on the cubes, which have ∼55% selectivity to produce crotonaldehyde at 200 °C (Figure 5). On the wires, crotonaldehyde production exhibits two maxima near 150 and 275 °C with a selectivity of ∼50% for crotonaldehyde at 200 °C (Figure 5). On the octahedra, the crotonaldehyde selectivity is comparable to the cubes and wires near 200 °C, but dramatically increases at $T > T_{10}$, compared to the other shapes (Figure 4). The formation of crotonaldehyde through an aldol condensation reaction should produce one equivalent of H_2O, and the initial maximum in the water profile correlates well with the maxima of the crotonaldehyde evolution on each nanoshape. At $T < T_{10}$, ethanol and crotonaldehyde are formed with similar selectivities on the cubes and wires, with 2−4 times higher selectivity for crotonaldehyde, compared to ethanol. However, the octahedra have ∼10 times higher selectivity for crotonaldehyde than ethanol at 200 °C, and ∼25 times higher selectivity for crotonaldehyde than ethanol at $T > T_{10}$. Interestingly, the nanoshapes also produce reduced and/or deoxygenated coupling products at $T < T_{10}$ with selectivities of <5%, namely, crotyl alcohol, 1,3-butadiene, and 2-butene. Water formation could also occur via dehydration of acetaldehyde to produce acetylene or, if surface H is available, ethylene. However, neither ethylene nor acetylene is observed in TPD or TPSR. These products may not form; or their intermediates may remain on the surface and contribute to the deactivation of the catalysts.

When $T > T_{10}$, there is a greater consumption of acetaldehyde on all shapes. The amount of acetaldehyde in the product stream at 425 °C is decreased by ∼25%, 70%, and 10% from its initial concentration for the cubes, wires, and octahedra, respectively. The cubes and wires have a reduced selectivity for crotonaldehyde, less ethanol is desorbed, and the amount of coupling products such as crotyl alcohol and 2-butene formed in this region increases. In addition, there is increased evolution of products that are associated with the scission of C−C bonds, including methane, CO, CO_2, and acetone. The onset of methane evolution begins at $T < T_{10}$ for all the nanoshapes and the selectivity to produce methane at $T > T_{10}$ on the cubes and wires increases, compared to $T < T_{10}$. However, no such increase in selectivity is observed on the octahedra. The amount of CO_2 and CO produced on cubes, wires, and octahedra is still increasing at 425 °C. H_2O, which can form from dehydration, Aldol condensation, or surface reduction, also maximizes at 425 °C for all three nanoshapes. No evolution of O_2 is observed on any of the nanoshapes. Despite significant acetate formation indicated in TP-DRIFTS (especially on the cubes), neither acetic acid nor formic acid, possible oxidation products, were observed. Also, no ethylene, a possible direct dehydration product, was observed for any of the nanoshapes.

Surprisingly, several cyclic products (≲5% selectivity between 100 and 400 °C) were evolved from the nanoshapes, including toluene, benzene, and furan (see Figure S2 in the Supporting Information). Furan is formed at $T < T_{10}$ on all nanoshapes. Ring closure of crotonaldehyde to form furan would create one equivalent of H_2. H_2 formation is observed throughout the

dx.doi.org/10.1021/cs500611g | ACS Catal. 2014, 4, 2437−2448

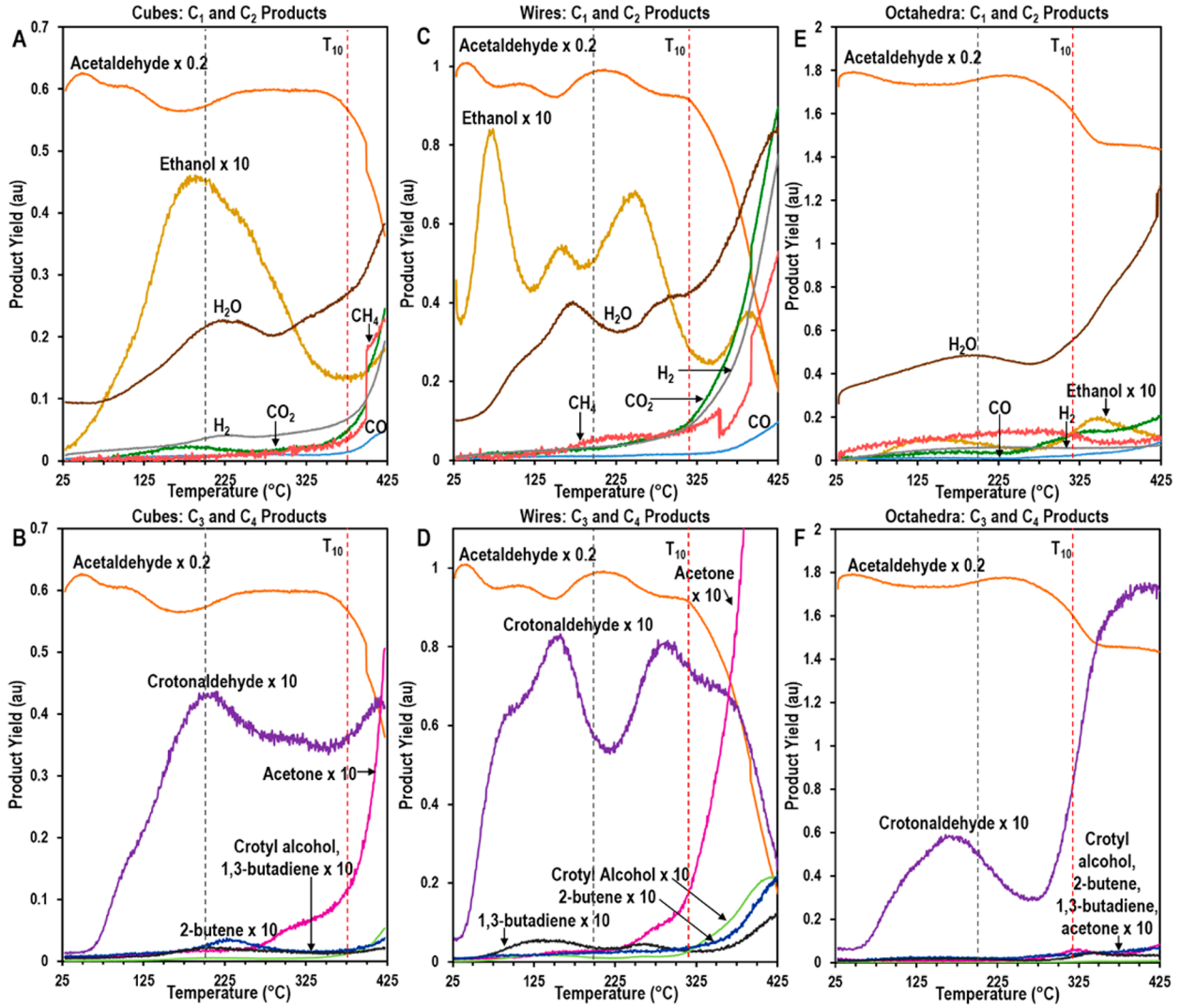

Figure 4. Temperature-programmed surface reaction (TPSR) profiles under a constant acetaldehyde stream for CeO_2 ((A, B) cubes, (C, D) wires, and (E, F) octahedra). Products are separated by C_1−C_2 products and C_3−C_4 products and the MS intensity is scaled as indicated for clarity. The conversion increases significantly above T_{10} (red dashed lines, see text). The product distributions in Figure 5 are taken from T = 200 °C, indicated by the black dashed lines.

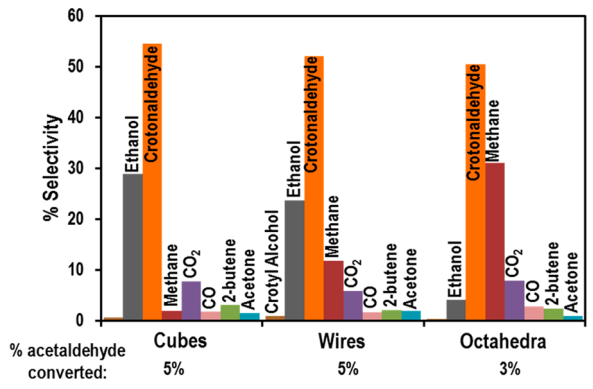

Figure 5. Product selectivities at 200 °C obtained from analysis of the TPSR profiles (see the Experimental Section) and compared for the three nanoshapes. Unconverted acetaldehyde constitutes the majority component of the product stream, and the total acetaldehyde conversion at 200 °C is indicated.

entire TPSR temperature range for all the nanoshapes. Similar to crotonaldehyde production, the evolution of furan is delayed by ∼30 °C in the cubes and octahedra compared to the wires. In contrast, benzene and toluene are only observed at $T > T_{10}$, and their evolution is closely correlated to the increase in formation of 2-butene, 1,3-butadiene, and acetone as the energy barrier to promote multiple reaction pathways is overcome.

The generation of products as a result of multiple coupling reactions may result in deactivation of the catalyst. Coupling products with high molecular weights have low volatility and may bond strongly to the oxide, poisoning the surface, and will therefore not be detected by MS. Indeed, at the end of TPSR, the wire and cubes had significant amounts of oily brown-black residue on the quartz U-tube and for all catalysts shapes, the catalyst changed from a whitish-yellow color to a brown color. Heating the catalysts in O_2/He at 400 °C for 1 h caused the catalyst to revert to its original color. Repeating the TPSR experiments with the O_2/He-treated catalysts resulted in good reproducibility of the TPSR results. In addition, examination of the catalysts via SEM after TPSR and O_2/He treatment showed that the catalysts retained their original morphology.

Isothermal Reaction and Deactivation. In order to better quantify the reaction selectivity and amount of

dx.doi.org/10.1021/cs500611g | ACS Catal. 2014, 4, 2437−2448

acetaldehyde converted at different temperatures and times-on-stream, reactions were run under isothermal conditions, and the reactor eluent was analyzed using GC with FID and TCD. The sample masses were adjusted to have the same total surface area. To probe the product selectivity under isothermal conditions, the product stream was analyzed after 11 min of continuous flow of acetaldehyde over a fresh catalyst at the indicated temperatures. The primary product observed in the eluent was crotonaldehyde for all nanoshapes at 100, 200, and 300 °C (see Table S2 in the Supporting Information), but at 400 °C, the methane, acetone, and carbon oxides become significant (Table 2).

Table 2. Isothermal Reactivity of Nanoshapes for Consumption of Acetaldehyde at 400 °C Collected after 11 Min, Corrected for the Carbon Number[a]

	Selectivity (%) at T = 400 °C		
	cubes	wires	octahedra
acetaldehyde consumed	60	94	36
crotonaldehyde	4	8	17
methane	2	3	<1
acetone	5	15	<1
CO and CO_2	3	11	<1
ethanol	1	1	<1
unassigned	5	5	2
carbon capture	40	50	15

[a]Product selectivities are given as a percentage of the inlet acetaldehyde. Reaction is based on the equivalent total surface area of 1.43 m^2 for the three ceria samples.

Figure 6 shows the *consumption* of acetaldehyde versus temperature for the three shapes. A portion of the inlet acetaldehyde is converted to products that desorb, but also a significant amount is captured on the catalysts. From measurements of the decrease of acetaldehyde and analysis of all products, the fraction of acetaldehyde that remains on the sample is deduced (see the Experimental Section) and is shown as dashed lines in Figure 6. The amount retained on the surface is especially significant at 400 °C for all nanoshapes. The buildup of carbonaceous residue on the surface results in catalyst deactivation and complicates the analysis of reaction kinetics.

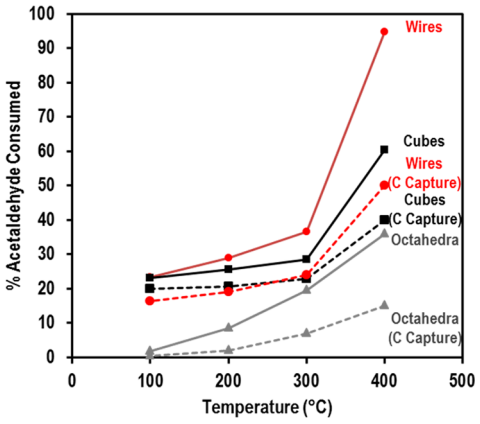

Figure 6. Acetaldehyde consumed after 11 min of constant acetaldehyde flow versus the temperature for CeO_2 wires, cubes, and octahedra (solid lines). The portion of consumption that leads to carbonaceous buildup (C Capture) is shown for CeO_2 wires, cubes, and octahedra (dotted lines). The sample masses were adjusted to have the same total surface area, equal to 1.43 m^2.

The product stream was also sampled at times after 11 min, but it was found that acetaldehyde conversion dropped rapidly, indicating the effects of catalyst deactivation. Shown in Figure 7 is the decrease in the consumption (conversion and capture) of acetaldehyde versus time-on-stream at 400 and 300 °C. The sample masses were adjusted to have the same total surface area. At 400 °C, the wires have the highest conversion, but also a high rate of deactivation with a 74% decrease in activity over 60 min. Cubes have a similarly high rate of deactivation at 400 °C, with a 75% decrease in activity that primarily occurs in the first 20 min of the reaction. Octahedra have the lowest rate of deactivation, with a 33% decrease over 60 min. At 300 °C, the wires and the cubes again have high initial rates of deactivation, with the acetaldehyde consumption rate decreasing 62% and 86%, respectively, over 60 min. Again, the octahedra have the lowest deactivation, with the acetaldehyde consumption decreasing 40% over 60 min. It is expected that co-feeding O_2, CO_2, or H_2O may decrease the amount of deactivation, and this will be the subject of future studies.

DISCUSSION

TP-DRIFTS data indicate that acetaldehyde adsorbs in the η^1-conformation at room temperature on the cubes and octahedra. This interaction is relatively weak, and much of acetaldehyde adsorbed in this way will simply desorb rather than react as the temperature is increased. Previously, the adsorption and reaction of acetaldehyde was studied on oxidized and reduced $CeO_{2-x}(100)$ and $CeO_{2-x}(111)$ thin films using TPD, reflection absorption IR, soft x-ray photoelectron spectroscopy and near edge x-ray absorption fine structure, with acetaldehyde initially being introduced to the catalyst below room temperature.[16−18] For these films studied in a UHV environment, acetaldehyde adsorbed in the η^1-configuration on the fully oxidized (111) films. Upon reduction of the surface, vacancies on $CeO_{2-x}(111)$ thin films adsorb acetaldehyde to form enolate species. Without these vacancies, acetaldehyde primarily desorbs without undergoing reaction and coupling products are not observed.[16] However, on both oxidized and reduced $CeO_{2-x}(100)$ thin films, acetaldehyde adsorbs in a μ-C,O-acetaldehyde conformation (dioxyethylene) that dehydrogenates above 100 °C to form acetate and enolate species. Formation of μ-C,O-acetaldehyde is attributed to lower coordination of both O and Ce on the fully oxidized (100) surface.[18] The DFT-calculated IR spectrum for μ-C,O-acetaldehyde predicts a peak at 1002 cm^{-1} on $CeO_2(111)$.[16] Such a peak is not clearly observed on the nanoshapes, but could be slightly shifted and/or overlapping the modes for another species (ethoxide) on the surface and therefore cannot be eliminated as a possible bonding motif for acetaldehyde.

The enolate is expected to be a key intermediate for coupling reactions (Scheme 2).[38] Indeed, at room temperature, enolate peaks are observed on the cubes and possibly on the octahedra above 200 °C, and coupling products are produced both in TPD and TPSR for all nanoshapes. Enolate is expected to form on CeO_2 octahedra with {111} facets if vacancies are present, based on previous reports.[16] Surface vacancies could form from the low-temperature water desorption observed on wires and octahedra, or may be present at the edges and corners.

Compared to the cubes, the wires show less enolate and more coupling products, as indicated by the low-frequency

dx.doi.org/10.1021/cs500611g | ACS Catal. 2014, 4, 2437−2448

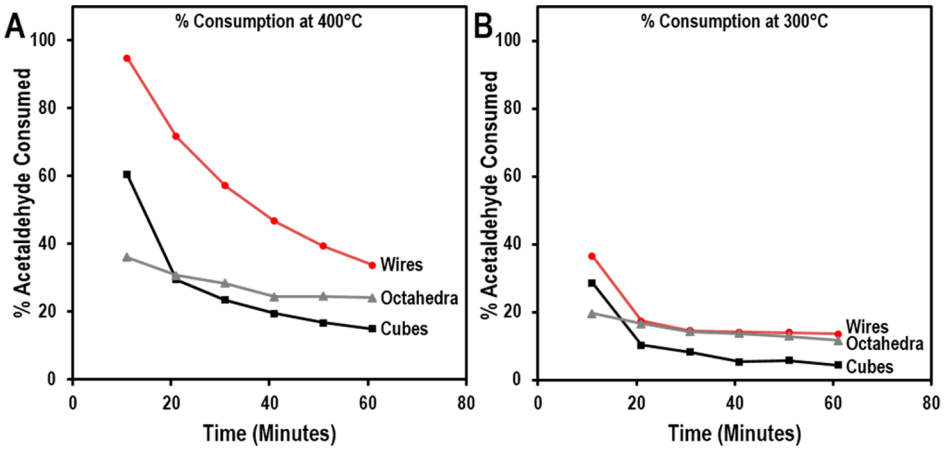

Figure 7. Percent consumption of acetaldehyde by CeO_2 cubes, wires, and octahedra over 1 h at (A) 400 °C and (B) 300 °C. The sample masses were adjusted to have the same total surface area, equal to 1.43 m^2.

Scheme 2. Proposed Mechanism for the Formation of Crotonaldehyde from the Adsorption and Reaction of Acetaldehyde Shown for Example on a CeO_2 {111} Facet (Not to Scale)[a]

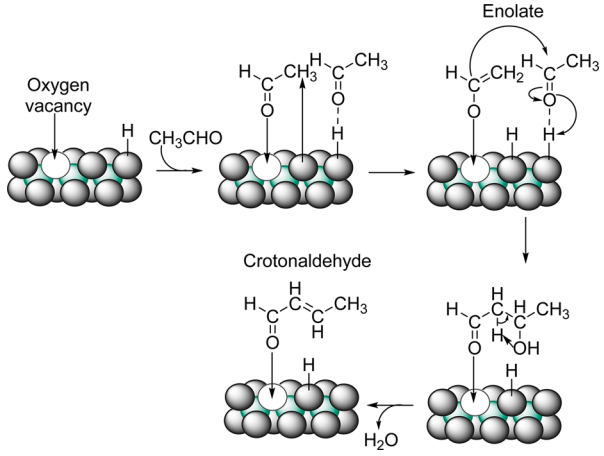

[a]Green spheres represent Ce atoms, gray spheres represent O atoms, and white circles denote oxygen vacancies.

υ(C═O) modes (1629 cm^{-1}). One explanation for the relative lack of enolate is that it may undergo reaction at or below room temperature and elude detection by FTIR. Adsorption below room temperature may be required to isolate the enolate. Indeed, the temperature as well as coverage may have a significant effect on the reaction of acetaldehyde on CeO_2. For the nanoshapes under reactor environment, coupling can occur readily upon adsorption of acetaldehyde at room temperature, even on the {111} faceted octahedra. Therefore, the increased number of defects, surface coverage, and the adsorption temperature on CeO_2 nanoshapes may contribute to the observed differences in adsorption and reactivity, compared to the single-crystalline films observed under UHV conditions.

Upon its formation, enolate can react with a second molecule of acetaldehyde and undergo an Aldol condensation reaction to form crotonaldehyde and 1 equiv of H_2O (Scheme 2).[11,18,35] Notably, this is the dominant coupling product observed in the product stream in TPSR. However, other coupling products are evolved from the cubes and wires at $T < T_{10}$, including 1,3-butadiene and 2-butene. Formation mechanisms are suggested in Scheme 3. Based upon the proposed mechanisms, one reason for the selectivity to crotonaldehyde may be that the

Scheme 3. Proposed Mechanism for the Formation of Several Coupling Products Evolved Shown for Example on CeO_2{111} Facet (Not to Scale)[a]

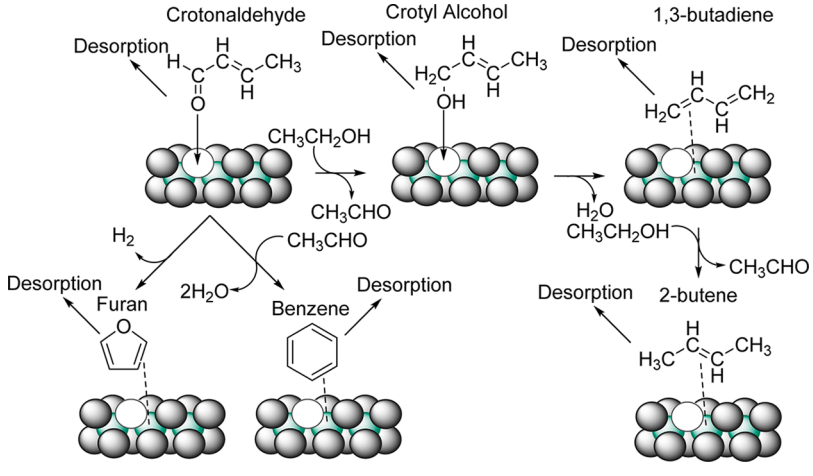

[a]Green spheres represent Ce atoms, gray spheres represent O atoms, and white circles denote oxygen vacancies.

dx.doi.org/10.1021/cs500611g | ACS Catal. 2014, 4, 2437−2448

formation of various coupling products must first proceed through a crotonaldehyde intermediate, which can desorb rather than undergo further reaction (Scheme 3). In support of this hypothesis, it is noted that the crotonaldehyde is produced at a lower onset temperature than the other coupling products, including, 1,3-butadiene, 2-butene, and crotyl alcohol. Crotyl alcohol is formed upon the reduction of crotonaldehyde, and it is only produced above 375 °C on the cubes and above 320 °C on the wires with <4% selectivity. The small amount of crotyl alcohol could be related to the lack of available H necessary to reduce the crotonaldehyde. Another possibility is that crotyl alcohol dehydration to 1,3-butadiene is rapid (see Step 2 in Scheme 3).

Rapid dehydration of crotyl alcohol is a key factor in the Lebedev and Ostromislensky processes.[39−41] In the Lebedev process, ethanol is used as a starting material to form 1,3-butadiene. The reaction proceeds through a crotyl alcohol intermediate that undergoes dehydration to form 1,3-butadiene.[42−44] The Ostromislensky process is similar but uses acetaldehyde and ethanol to form 1,3-butadiene via a crotyl alcohol intermediate.[40,44] If there is excess ethanol in the system, it could favor the further reduction of 1,3-butadiene to form 2-butene and 1 equiv of acetaldehyde, as shown in Scheme 3. Indeed, butene was found to be a byproduct in the reaction of ethanol and acetaldehyde to produce 1,3-butadiene.[41] At $T < T_{10}$, it appears that dehydration of crotyl alcohol is favored since 1,3-butadiene and 2-butene are evolved on the wires and cubes, respectively, but not crotyl alcohol. However, at $T > T_{10}$, crotyl alcohol desorption becomes more favorable, compared to dehydration to 1,3-butadiene on the cubes and wires. It should be noted that crotyl alcohol and 1,3-butadiene are only observed when ethanol is present. On the octahedra, the only coupling product observed in TPSR is crotonaldehyde. According to Scheme 3, the formation of crotyl alcohol (and, hence, 1,3-butadiene) is limited by ethanol, which is needed for the reduction of crotonaldehyde.

Ethanol is observed in amounts that vary for cubes, wires, and octahedra. Barteau et al. reported that ethanol could be produced on $TiO_2(001)$ surfaces upon adsorption of acetaldehyde by reacting with surface H, which is a direct reduction.[45] However, Mullins et al. reported that no ethanol was observed on $CeO_2(100)$ single-crystalline thin films upon adsorption of acetaldehyde, even upon dissociative adsorption of water on the surface.[18] A Cannizzaro disproportionation of two acetaldehyde molecules would result in the formation of ethoxy and acetate groups (Scheme 1). In this base-catalyzed reaction, surface O can perform a nucleophilic attack on the carbonyl of an aldehyde molecule, followed by a hydride transfer to a second molecule of adsorbed aldehyde to form the alkoxy. This pathway has been proposed for alcohol formation from formaldehyde adsorption on $CeO_{2-x}(111)$,[46] MgO, and $TiO_2(001)$ films,[47−49] and acetaldehyde adsorption on rutile TiO_2.[34] Alkoxy can combine with hydrogen from a surface-bound hydroxyl to desorb as the alcohol. We propose that this disproportionation is the primary route to ethanol on all shapes. Within this mechanism, the dependence on surface structure in the production of ethanol would be related to the base strength of the surface oxygen that performs the nucleophilic attack.[48] Higher ethanol production (and surface acetate) on cubes compared to octahedra implies a more basic character in (100) than (111). Therefore, the basicity of the surface is a significant factor in the structure-dependent selectivity.

When $T > T_{10}$, C−C bond scission becomes more favorable, resulting in the increased production of various C_1 products, such as CO, CO_2, and methane, but also the coupling products acetone and toluene. Bond energies for a free acetaldehyde molecule are 96 kcal/mol for the acetyl C−H bond, 177.3 kcal/mol for the C═O bond, 84.4 kcal/mol for the C−C bond, and 99 kcal/mol for the methyl C−H bonds.[50] While the C−C bond is the weakest, the interaction of the acetyl O with the CeO_2 catalyst modifies the electron density and, therefore, the bond energies. The room-temperature formation of crotonaldehyde suggests that it is easier to break the methyl C−H bond, and the C═O bond, than the C−C bond. In comparison, CO_2 formation, which requires C−C bond scission, only occurs at temperatures above 125 °C for all shapes.

It has been suggested that the production of acetone occurs via ketonization of two acetate groups.[11] Therefore, it is unique among the coupling products in that it would not be expected to proceed through an enolate intermediate. The acetate groups can form via oxidation of acetaldehyde or a Cannizzaro disproportionation reaction. Subsequently, the acetates can undergo ketonization to form acetone and 1 equiv of CO_2, formally leaving a surface O atom. This O atom may assume a lattice site or, if surface H is available, the O atom could form OH or desorb as H_2O. Indeed, water evolution increases concurrently with acetone formation. The ability to promote the oxidation of acetaldehyde to produce acetate species is related to the basicity of the surface. A higher basicity has been reported to correlate to a more ionic surface, which would be able to donate electron density from surface O to the α-carbon of acetaldehyde, therefore oxidizing the acetaldehyde and leading to acetate groups.[12] The cubes displayed bands associated with acetate groups (and the octahedra, to a lesser extent) in the TP-DRIFTS. However, the wires produce a large amount of acetone in the TPD, compared to the small amounts observed on the cubes and none on the octahedra. In the integrated TPD, TPSR, and isothermal reactions at higher temperatures, acetone production is ranked in the following order: wires > cubes ≫ octahedra. Because acetate species are not observed on the wires by DRIFTS, yet acetone is clearly produced, this result could suggest that acetate is consumed rapidly upon formation. The primary reason for the lack of acetone product from octahedra is attributed to the relatively low surface coverage of acetate caused by the lower base strength predicted for the {111} surfaces.

In addition to undergoing ketonization to form acetone, acetate groups can also undergo C−C bond scission to form the C_1 products methane, CO_2, and CO, depending on the selectivity between hydrogenation or dehydrogenation pathways and the amount of accessible surface O and H. Notably, at 400 °C in TPSR, the nanoshapes display different selectivities to form these products. The CO_2:CO selectivity ratio in TPSR is ∼2, 5, and 10, for the octahedra, cubes, and wires, respectively (see Figure S2 in the Supporting Information). This result suggests that it is easier to remove oxygen from the surface of the wires and cubes than the octahedra, and is likely related to the lowest oxygen vacancy formation energies for the {111} surface. At $T > T_{10}$, the C−C bond scission, ketonization, and coupling occur concurrently, as indicated by the coevolution of C_1 products, acetone, and crotonaldehyde, respectively, which is clearly seen in TPSR (Figure 4) and isothermal experiments (see Table S2 in the Supporting Information). However, the distribution of these products is very shape-sensitive. Roughly, octahedra produce more

dx.doi.org/10.1021/cs500611g | ACS Catal. 2014, 4, 2437−2448

crotonaldehyde, compared to C_1 and acetone; cubes produce more C_1 and crotonaldehyde, compared to acetone; wires produce more CO_2 and acetone, compared to crotonaldehyde (see Figure S2 and Table S2 in the Supporting Information).

Cyclic products such as furan, benzene, and toluene are also observed. Furan has been observed previously from reaction of acetaldehyde on β-UO_3.[51] Furan selectivity is low for all nanoshapes (<5%) and its evolution is expected to occur from the dehydrogenation of crotonaldehyde (Scheme 3). At low temperature T in TPSR, its evolution coincides approximately with the onset of crotonaldehyde on all nanoshapes, but at $T > T_{10}$, it increases at the expense of crotonaldehyde on the wires. Benzene and toluene are primarily observed when $T > T_{10}$ (see Figure S3 in the Supporting Information). Benzene formation could occur via the addition of an acetaldehyde molecule to crotonaldehyde, forming 2 equiv of water and 1 equiv of benzene (Scheme 3). Benzene has been observed as a product on TiO_2, Al_2O_3, UO_2 (111), and CeO_2 previously, and been proposed to form via this mechanism.[35,52] Toluene has not previously been reported as a product on CeO_2 from the catalysis of acetaldehyde, however, it could be formed from the addition of a methyl group to benzene, in a mechanism similar to that of acetone.[11] The polymerization of acetaldehyde to form high-molecular-weight species that do not easily desorb could contribute to the deactivation of the catalyst. Indeed, catalyst deactivation is a significant problem in the Lebedev and Ostromislensky processes, with the amount of polymerization increasing as the amount of acetaldehyde used in the reaction was increased.[41] Notably, a large amount of carbonaceous material is calculated to be retained on the surfaces of the various products (see Table 2 and Figure 6) and likely contributes to the deactivation that is observed for the various nanoshapes (Figure 7).

Differences between the nanoshapes in selectivity, acetaldehyde consumption, and deactivation were also observed utilizing isothermal reactions. For example, at 400 °C (Table 2 and Figure 6), wires give the highest consumption rates of acetaldehyde (94%). Yet, the wires produce a low ratio (1:4) of crotonaldehyde, relative to the sum of the other products, including acetone, ethanol, CO, and CO_2. In contrast, the octahedra produce a higher ratio of crotonaldehyde to the sum of the other products (4:1). This higher selectivity to produce crotonaldehyde over other products is countered by having lower acetaldehyde consumption (36%). Finally, the cubes produce a ratio of crotonaldehyde to the sum of the other products of 1:4, similar to wires, but the amount of acetaldehyde consumed is 60%. Significantly, the ethanol selectivity was lower in isothermal experiments compared to TPSR experiments. These differences in the product selectivity could be related to factors such as different reaction times and temperatures of initial exposure for the respective experiments that result in variations in the amounts and types of surface intermediates and carbonaceous buildup. Thus, the reaction conditions and time-on-stream are significant factors in determining the selectivity.

The differences in how acetaldehyde adsorbs and reacts are likely to be related to the basicity of the different surfaces, since more basic surface oxygen groups would favor ethanol (and acetate) formation. However, other parameters likely contribute to the observed reactivity, including the coordination numbers of surface Ce and O species, as well as the varying defect nature of the nanoshapes. The theoretical coordination numbers vary depending on the surface facets. Ce atoms on {100} and {110} surfaces have a theoretical coordination number of 6, while Ce atoms on {111} surfaces have a theoretical coordination number of 7. O atoms on {111} and {110} surfaces have a theoretical coordination number of 3, while O atoms on {100} surfaces have a theoretical coordination number of 2. A lower coordination number would be expected to correlate to a higher reactivity and overall mirrors the higher reactivity observed in the cubes with {100} facets, compared to octahedra with {111} facets.[53] In addition, it was previously reported that CeO_2 rods and cubes had greater surface O-vacancy densities, compared to CeO_2 octahedra, and that CeO_2 rods had more clustered defects than CeO_2 cubes or octahedra.[54] Defects are high-energy sites and can be responsible for higher or unique reactivity, although they are minority sites on the cubes and octahedra. In particular, O-vacancy sites have been shown to be the active sites for dissociative adsorption of methanol and acetaldehyde on CeO_{2-x}.[17,55] Therefore, the conversion of acetaldehyde on CeO_2 is likely enhanced by clusters of vacancies and defects and promotes the formation of enolate species upon acetaldehyde adsorption.

CONCLUSIONS

Herein, shape-controlled CeO_2 nanoshapes with well-defined surface crystallographic orientations were used to evaluate the structure-dependent properties for the adsorption and reaction of acetaldehyde. Rich catalytic chemistry is observed, including coupling reactions (to crotonaldehyde, crotyl alcohol, 1,3-butadiene, 2-butene), ketonization (to acetone), Cannizzaro disproportionation (to ethanol and acetate), ring closure (to furan and benzene), and C−C bond scission (to methane and CO_2 or CO). Differences are observed in the reaction selectivity, surface species, and desorption products, among the different nanoshapes. These differences are attributed to structure-related variation in defect density, surface oxygen coordination, vacancy formation energy, and acid/base properties. Although rapid deposition of carbonaceous material on the surface occurs, thereby altering the surface chemistry, the following trends in structure−reactivity are observed:

- Reactive coupling of acetaldehyde to produce crotonaldehyde occurs by Aldol condensation on all nanoshapes, but with higher selectivity on the octahedra at 400 °C in TPSR and isothermal reactions.
- Enolate is observed by DRIFTS only on the cubes, but it is the believed to be a short-lived intermediate in the Aldol condensation to crotonaldehyde observed on all shapes.
- Ethanol is formed by a Cannizzaro disproportionation in TPD and TPSR leaving acetate; wires ≈ cubes ≫ octahedra. Higher base strength of defects and {100} surfaces leads to the activation of acetaldehyde to initiate this reaction.
- Similarly, decreased acetone production from octahedra compared to cubes and wires in TPD, TPSR, and isothermal reaction is attributed to the relative lack of surface acetate caused by the lower base strength predicted for the {111} surfaces, compared to {100} and defects.
- C−C bond scission of acetate leads to correlated evolution of CO, CO_2, and methane above 400 °C in TPSR on all shapes, with a selectivity at 400 °C that ranks in the following order: wires ≈ cubes ≫ octahedra. This ordering is attributed to lower coverage of acetate on the octahedra.
- Desorption of crotonaldehyde from the less-reactive {111} facets of octahedra, in comparison with the increased activation of adsorbates on defects and active {100} surfaces, may explain

dx.doi.org/10.1021/cs500611g | ACS Catal. 2014, 4, 2437−2448

the lower rates of coking on the octahedra, compared to wires and cubes.

■ ASSOCIATED CONTENT

Supporting Information

Scheme for monodentate and bidentate ethoxide; SEM, TEM, and XRD of synthesized CeO_2 nanoshapes; percent selectivities for TPSR, TPSR-MS profiles for cyclic products; percent composition of C-containing product stream for TPD by MS; isothermal selectivity for the nanoshapes by GC. This material is available free of charge via the Internet at http://pubs.acs.org.

■ AUTHOR INFORMATION

Corresponding Author

*E-mail: overburysh@ornl.gov.

Present Address

[†]Fritz Haber Institute Max Planck, Faradayweg 4−6, 14195 Berlin, Germany.

Notes

The authors declare no competing financial interest.

■ ACKNOWLEDGMENTS

This research is sponsored by the Division of Chemical Sciences, Geosciences, and Biosciences, Office of Basic Energy Sciences, U.S. Department of Energy. Part of the work including synthesis, XRD, TEM, and SEM was conducted at the Center for Nanophase Materials Sciences, which is sponsored at Oak Ridge National Laboratory by the Scientific User Facilities Division, Office of Basic Energy Science, U.S. Department of Energy.

■ REFERENCES

(1) Kašpar, J.; Fornasiero, P.; Graziani, M. *Catal. Today* **1999**, *50*, 285−298.
(2) Shido, T.; Iwasawa, Y. *J. Catal.* **1992**, *136*, 493−503.
(3) Jasinski, P.; Suzuki, T.; Anderson, H. U. *Sens. Actuators, B* **2003**, *95*, 73−77.
(4) Beie, H. J.; Gnörich, A. *Sens. Actuators, B* **1991**, *4*, 393−399.
(5) Park, S.; Vohs, J. M.; Gorte, R. J. *Nature* **2000**, *404*, 265−267.
(6) Vivier, L.; Duprez, D. *ChemSusChem* **2010**, *3*, 654−678.
(7) Li, M.; Wu, Z.; Overbury, S. H. *J. Catal.* **2013**, *306*, 164−176.
(8) Senanayake, S. D.; Mullins, D. R. *J. Phys. Chem. C* **2008**, *112*, 9744−9752.
(9) Lykhach, Y.; Happel, M.; Johánek, V.; Skála, T.; Kollhoff, F.; Tsud, N.; Dvořák, F.; Prince, K. C.; Matolín, V.; Libuda, J. *J. Phys. Chem. C* **2013**, *117*, 12483−12494.
(10) Wu, Z.; Li, M.; Overbury, S. H. *J. Catal.* **2012**, *285*, 61−73.
(11) Idriss, H.; Diagne, C.; Hindermann, J. P.; Kiennemann, A.; Barteau, M. A. *J. Catal.* **1995**, *155*, 219−237.
(12) Kydd, R.; Teoh, W. Y.; Scott, J.; Ferri, D.; Amal, R. *ChemCatChem.* **2009**, *1*, 286−294.
(13) Mavrikakis, M.; Barteau, M. A. *J. Mol. Catal. A: Chem.* **1998**, *131*, 135−147.
(14) Ren, H.; Yu, W.; Salciccioli, M.; Chen, Y.; Huang, Y.; Xiong, K.; Vlachos, D. G.; Chen, J. G. *ChemSusChem* **2013**, *6*, 798−801.
(15) Alonso, D. M.; Bond, J. Q.; Dumesic, J. A. *Green Chem.* **2010**, *12*, 1493−1513.
(16) Calaza, F. C.; Xu, Y.; Mullins, D. R.; Overbury, S. H. *J. Am. Chem. Soc.* **2012**, *134*, 18034−18045.
(17) Chen, T. L.; Mullins, D. R. *J. Phys. Chem. C* **2011**, *115*, 3385−3392.
(18) Mullins, D. R.; Albrecht, P. M. *J. Phys. Chem. C* **2013**, *117*, 14692−14700.
(19) Feng, X.; Sayle, D. C.; Wang, Z. L.; Paras, M. S.; Santora, B.; Sutorik, A. C.; Sayle, T. X. T.; Yang, Y.; Ding, Y.; Wang, X.; Her, Y.-S. *Science* **2006**, *312*, 1504−1508.
(20) Kepenekçi, Ö.; Emirdag-Eanes, M.; Demir, M. M. *J. Nanosci. Nanotechnol.* **2011**, *11*, 3565−3577.
(21) Tana; Zhang, M.; Li, J.; Li, H.; Li, Y.; Shen, W. *Catal. Today* **2009**, *148*, 179−183.
(22) Yan, L.; Yu, R.; Chen, J.; Xing, X. *Cryst. Growth Des.* **2008**, *8*, 1474−1477.
(23) Guo, Z.; Du, F.; Li, G.; Cui, Z. *Inorg. Chem.* **2006**, *45*, 4167−4169.
(24) Sun, C.; Li, H.; Chen, L. *Energy Environ. Sci.* **2012**, *5*, 8475−8505.
(25) Sun, C.; Li, H.; Chen, L. *J. Phys. Chem. Solids* **2007**, *68*, 1785−1790.
(26) Baudin, M.; Wójcik, M.; Hermansson, K. *Surf. Sci.* **2000**, *468*, 51−61.
(27) Mai, H.-X.; Sun, L.-D.; Zhang, Y.-W.; Si, R.; Feng, W.; Zhang, H.-P.; Liu, H.-C.; Yan, C.-H. *J. Phys. Chem. B* **2005**, *109*, 24380−24385.
(28) Zhou, K.; Wang, X.; Sun, X.; Peng, Q.; Li, Y. *J. Catal.* **2005**, *229*, 206−212.
(29) Florea, I.; Feral-Martin, C.; Majimel, J.; Ihiawakrim, D.; Hirlimann, C.; Ersen, O. *Cryst. Growth Des.* **2013**, *13*, 1110−1121.
(30) Paier, J.; Penschke, C.; Sauer, J. *Chem. Rev.* **2013**, *113*, 3949−3985.
(31) Nolan, M.; Parker, S. C.; Watson, G. W. *Surf. Sci.* **2005**, *595*, 223−232.
(32) Wu, Z.; Li, M.; Mullins, D. R.; Overbury, S. H. *ACS Catal.* **2012**, *2*, 2224−2234.
(33) Gines, M. J. L.; Iglesia, E. *J. Catal.* **1998**, *176*, 155−172.
(34) Rekoske, J. E.; Barteau, M. A. *Langmuir* **1999**, *15*, 2061−2070.
(35) Raskó, J.; Kiss, J. *Appl. Catal., A* **2005**, *287*, 252−260.
(36) Takahashi, A.; Haneda, M.; Fujitani, T.; Hamada, H. *J. Mol. Catal. A: Chem.* **2007**, *261*, 6−11.
(37) Busca, G.; Lorenzelli, V. *Mater. Chem.* **1982**, *7*, 89−126.
(38) Singh, M.; Zhou, N.; Paul, D. K.; Klabunde, K. J. *J. Catal.* **2008**, *260*, 371−379.
(39) Makshina, E. V.; Janssens, W.; Sels, B. F.; Jacobs, P. A. *Catal. Today* **2012**, *198*, 338−344.
(40) Quattlebaum, W. M.; Toussaint, W. J.; Dunn, J. T. *J. Am. Chem. Soc.* **1947**, *69*, 593−599.
(41) Toussaint, W. J.; Dunn, J. T.; Jachson, D. R. *Ind. Eng. Chem.* **1947**, *39*, 120−125.
(42) Lebedev, S. V. *J. Gen. Chem.* **1933**, *3*, 698−708.
(43) Lebedev, S. V. British Patent 331402, 1929.
(44) Angelici, C.; Weckhuysen, B. M.; Bruijnincx, P. C. A. *ChemSusChem* **2013**, *6*, 1595−1614.
(45) Idriss, H.; Barteau, M. A. *Catal. Lett.* **1996**, *40*, 147−153.
(46) Zhou, J.; Mullins, D. R. *Surf. Sci.* **2006**, *600*, 1540−1546.
(47) Barteau, M. A. *Chem. Rev.* **1996**, *96*, 1413−1430.
(48) Peng, X. D.; Barteau, M. A. *Langmuir* **1989**, *5*, 1051−1056.
(49) Idriss, H.; Kim, K. S.; Barteau, M. A. *Surf. Sci.* **1992**, *262*, 113−127.
(50) Sanderson, R. *Chemical Bonds and Bonds Energy*; Academic Press: London, 2012; pp 200−201.
(51) Madhavaram, H.; Idriss, H. *Catal. Today* **2000**, *63*, 309−315.
(52) Chong, S. V.; Idriss, H. *J. Vac. Sci. Technol., A* **2001**, *19*, 1933−1937.
(53) Alghamdi, K.; Hargreaves, J. S. J.; Jackson, S. D. Base Catalysis with Metal Oxides. In *Metal Oxide Catalysis*; Jackson, S. D., Hargreaves, J. S. J., Eds.; Wiley−VCH: Weinheim, Germany, 2008; pp 819−843.
(54) Wu, Z.; Li, M.; Howe, J.; Meyer, H. M.; Overbury, S. H. *Langmuir* **2010**, *26*, 16595−16606.
(55) Namai, Y.; Fukui, K.-i.; Iwasawa, Y. *Nanotechnology* **2004**, *15*, S49.
(56) Li, C.; Sakata, Y.; Arai, T.; Domen, K.; Maruya, K.-i.; Onishi, T. *J. Chem. Soc., Faraday Trans. 1* **1989**, *85*, 929−943.